Rapid On-Demand Design of Inverted All-Dielectric Metagratings for Trace Terahertz Molecular Fingerprint Sensing by Deep Learning

Xueying Liu, [a,b,†] Yinong Xie, [a,†] Yiming Yan [a,†], Qiang Niu, [a] Li-guo Zhu, [c] Zhaogang Dong, [e,f] Qing Huo Liu,[a] and Jinfeng Zhu [a,*]

[a]Institute of Electromagnetics and Acoustics and Key Laboratory of Electromagnetic Wave Science and Detection Technology, Xiamen University, Xiamen, 361005, China

[b]Key Laboratory of Grain Information Processing and Control, College of Information Science and Engineering, Henan University of Technology, Zhengzhou 450001, China

[c]Microsystem and Terahertz Research Center, China Academy of Engineering Physics, Mianyang, Sichuan 621900, China

[d]P

[e]Institute of Materials Research and Engineering (IMRE), Agency for Science, Technology and Research (A*STAR), 2 Fusionopolis Way, Innovis #08-03, Singapore 138634, Republic of Singapore

[f]Department of Materials Science and Engineering, National University of Singapore, 9 Engineering Drive 1, 117575, Singapore

[*]E-mail: nanoantenna@hotmail.com

[†]These authors contributed equally to this work.

Abstract:

Metasurface design with a multiplexing scheme holds promise for enhancing trace detection of terahertz (THz) molecular fingerprints. Conventional designs rely on matching spectral resonance positions with fingerprints of trace analytes, which require laborious metastructure optimizations by performing massive optical simulations. Recently, deep learning (DL) has indicated great potential for designing metasurfaces. However, its design application for THz fingerprint metasurface sensors has barely been reported so far. Here, we present a DL architecture of a bidirectional neural network to design an inverted all-dielectric metagrating (IAM) for trace THz fingerprint sensing. Based on a given THz fingerprint spectrum, our DL design tool can flexibly customize the critical sensing structure of the metagrating with the corresponding resonance frequency. Combining the designed IAM with angle multiplexing, one can excite a sequence of guided-mode resonances in a wide THz band, which supports elevating the THz fingerprint detection performance on a flat sensing surface. The DL design is used to guide the fabrication and measurement of IAM for trace α-lactose sensing, where the experimental results demonstrate metasensing enhancement by 9.3 times and imply the fast and powerful capability of our design method. Our research will inspire more DL applications on quick on-demand designs for many other THz metadevices and metasystems.

Keywords: Terahertz spectroscopy; Inverted all-dielectric metagrating; Deep learning; Inverse design; Fingerprint detection

1. Introduction

Terahertz (THz) spectroscopy offers a non-destructive and label-free detection approach for many biological and chemical molecules,[1-5] due to their unique fingerprint absorption features in the THz spectra. [6, 7] In applications of THz trace sensing, the mismatch between THz wavelengths and sample sizes usually leads to weak detection signals, which hinders effective molecule identification.[8] In order to overcome this problem, researchers have designed various THz metasurface sensors and utilized their near-field effects to boost the detection performance.[9-15] Recently, the use of metasurface in combination with the multiplexing technique has been widely investigated for THz trace sensing, since it provides a powerful way to amplify the broadband THz fingerprint signals.[16-22] In general, the structural parameters of multiplexed metasurface sensors are designed based on the frequency match between the resonance position and fingerprint peaks of target analytes. This design approach usually demands for a series of redundant optical simulation and highly depends on the engineering experiences of metasurface researchers.

Nowadays, the design of metamaterials and metasurfaces is witnessing the significant advancements of using deep learning (DL).[23-27] DL can establish the correlation between metastructures and optical responses by the artificial neural network instead of solving Maxwell equations, and it can dramatically reduce the simulation consumption compared to conventional numerical methods. Many DL models have been developed in this research field, such as multilayer perceptron (MLP), convolutional neural network, generative adversarial network, transformer and so on.[28-34] They have been adopted to design many kinds of metasurfaces, which cover a broad electromagnetic spectrum, including visible light, infrared waves and microwaves.[35-38] Despite these progresses, the use of the DL scheme has been barely reported in the field of THz metasurfaces and metadevices, especially for the on-demand metasurface design on trace fingerprint sensing.

In this work, we build up a bidirectional neural network based on the divide-and-conquer strategy for the intelligent design of inverted all-dielectric metagrating (IAM) for multiplexed THz sensing of trace fingerprint. This approach facilitates the rapid inverse design and fabrication of IAM sensors according to the given fingerprint peaks of target analytes. In combination with the platform of angle multiplexing, the devices feature the uniform sensing on a flat surface and dramatically enhance THz trace detection of broadband fingerprint signals. This study will inspire DL applications on the design of more THz metadevices and metasystems.

2. Results and Discussion

2.1. Theoretical basis of IAM fingerprint sensor and deep learning model

The design of IAM is based on the use of silicon (Si) material only, as illustrated in **Figure** 1a. Its meta-atom contains a layer of inverted subwavelength periodic gratings and an above waveguide layer. There are four crucial structural parameters to determine the resonance posiotion, including the metastructure period (P), waveguide layer thickness (T), grating height (H), and grating duty cycle (F). Based on the designed IAM for a given target analyte, one can adopt the angle multiplexing mechasim to excite a number of spectra with high-quality resonances for trace metasensing based on the light excitation of transverse electric (TE) THz waves. These resonances can cover and enhance the broadband fingerprint signal of trace analyte by comparing the spectral changes before and after sample loading.

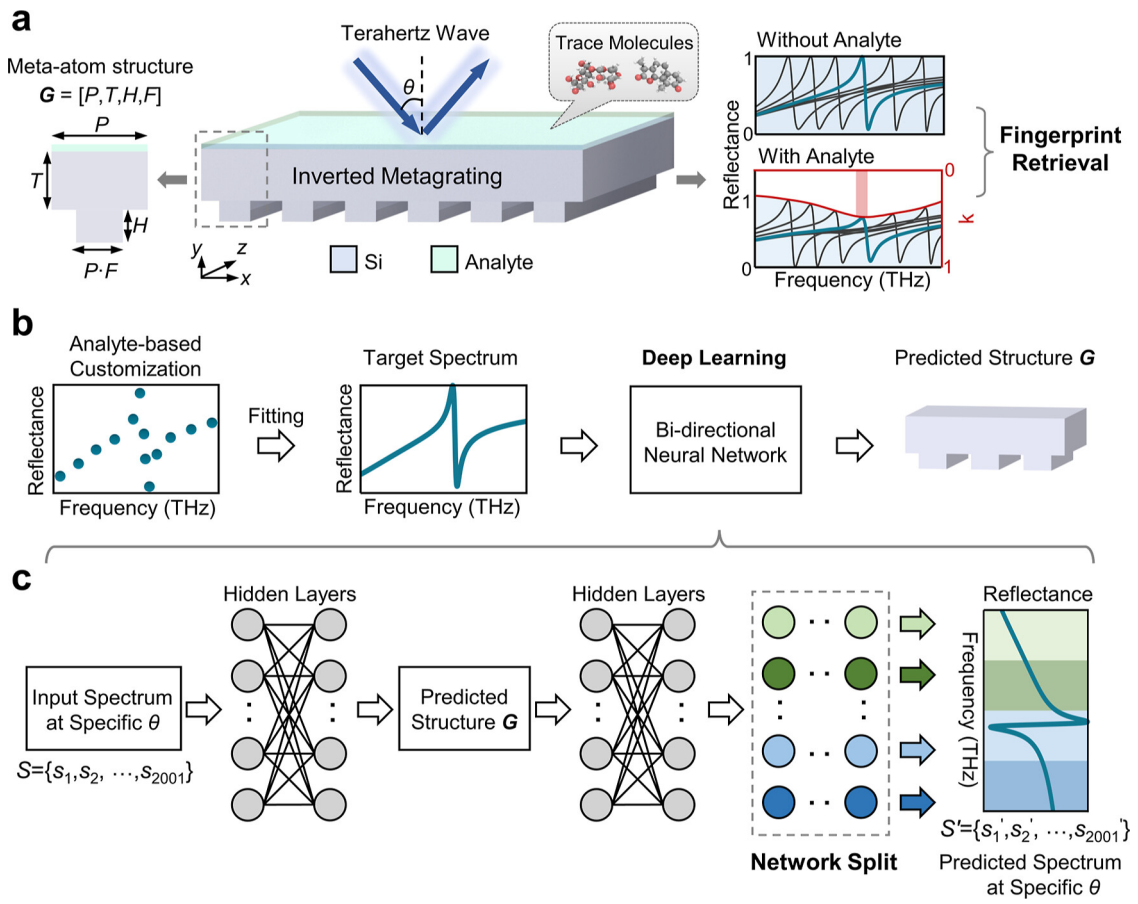

Figure 1. DL architecture of bidirectional NN to design an IAM for trace THz fingerprint sensing. (a) Schematic drawing of the IAM sensor and fingerprint retrieval by angle-multiplexing, where *G* = [*P*, *T*, *H*, *F*] denotes the metastructure geometry vector. The intensity change of angle-multiplexed reflected spectra before and after analyte loading is determined by its imaginary part *k* of complex refractive index. (b) Design process of the THz fingerprint metasensor. (c) Architecture of the DL model including the forward and inverse networks.

The process of DL design for the fingerprint metasensor is depicted in **Figure** 1b. It is established by a customer-defined design framework, which could generate an on-demand spectrum at a specific indicent angle for fingerprint sensing by freely moving a series of coordinate dots on the spectral layout. The generated spectrum is fitted by interpolation between the defined dots and used as the input target in the DL model. This model provides the real-time prediction of corresponding metastructure parameters. It adopts two sets of neural networks (NNs) based on MLP in order to accomplish the intelligent design of IAM sensor. The NNs are composed of the inverse and forward stages, as shown in **Figure** 1c. We input the

target spectrum into the inverse neural network (INN) to obtain the predicted metastructure parameters, which are used as the input for the forward neural network (FNN). The forward procedure is not only used to overcome misconvergence due to mapping of nonuniqueness, but also utilized to replace time-consuming simulation for validating INN design immediately [39-41]. Instead of predicting the entire spetrum by a single network, we propose a "divide-and-conquer" scheme, which employs multiple subnetworks to predict the spectrum in different wavelength ranges separately. This approach decomposes the prediction of a large problem into predictions of small problems and achieves better network performance. [32, 42, 43]

In the FNN, the vector S' has 2001 spectral sampling points with uniform space from 0.5 THz to 0.7 THz. It corresponds to the metastructure geometry vector G = [P, T, H, F], where 120 μm ≤ P ≤ 160 μm, 120 μm ≤ T ≤ 170 μm, 25 μm ≤ H ≤ 45 μm and 0.4 ≤ F ≤ 0.6. The sizes of fully connected layers in the spectrum-split FNN are 4, 2048, 2048, 2048, (2048/*j*, 2048/*j*, 2048/*j*, 2048/*j*, 2001/*j*)·*j*,[18] respectively, where *j* denotes the number of split subnetworks. Here we take *j* as 8. The inverse INN consists of 6 fully connected hidden layers with the sizes of 2001, 1024, 1024, 1024, 1024, 1024, 1024, 4, respectively. ReLU is used as the activation function in both networks. The Adam optimizer is applied for gradient descent. The loss function is based on the calculation of mean square error (MSE) between the predicted results and the ground truth from optical simulation, defined as the following equation,

$$\mathrm{Loss}_{FNN} = \frac{1}{N}\sum_{i=1}^{N}\left(S_i' - \tilde{S}_i\right)^2, \tag{1}$$

where S_i' is the sampling point of the spectrum predicted by FNN, $\tilde{S}_i$ denotes the sampling point of the simulated spectrum and N is the number of sampling points. The loss function of INN is also defined as the MSE between the predicted metastructure parameters and the ground truth.

2.2. DL model performance and on-demand design for angle-multiplexed IAM

Next, we evaluate the performance of proposed DL design method. We randomly select several test instances and analyze them in **Figure** 2. As shown in **Figure** 2a,b, the FNN predictions indicate the remarkable consistency with the ground truth from optical simulation, whether the spectrum has a single peak or multiple peak/valley features. For the metastructures with high-Q resonance, the FNN prediction demonstrates high accuracy for the peak position and shape. In fact, compared with the conventional FNN, the proposed FNN adopts the "divide-and-conquer" scheme in the MLP architecture and shows 34.1% reduction on MSE with 23% reduction of training parameters. These results illuminate the strong forward design capability of our method for on-demand metastructures with various geometric parameters. The prediction accuracy of INN are exhibited in **Figure** 2c,d by providing two randomly chosen design samples. Compared with the ground truth of metastructures, the absolute prediction errors of all three structural parameters P, T and H are less than 0.4 μm with the proportional errors lower than 0.27%. Meanwhile, the predictions for F are completely correct. The simulated spectra corresponding to the predicted structure parameters are highly consistent with the ground truth fed to the INN. The calculated MSE of INN is as low as 3.6×10^{-5}, incicating the high prediction accuracy from spectra to metastructures statistically. Therefore, our approach establishes a reliable DL architecture for both forward and inverse design of metastructures.

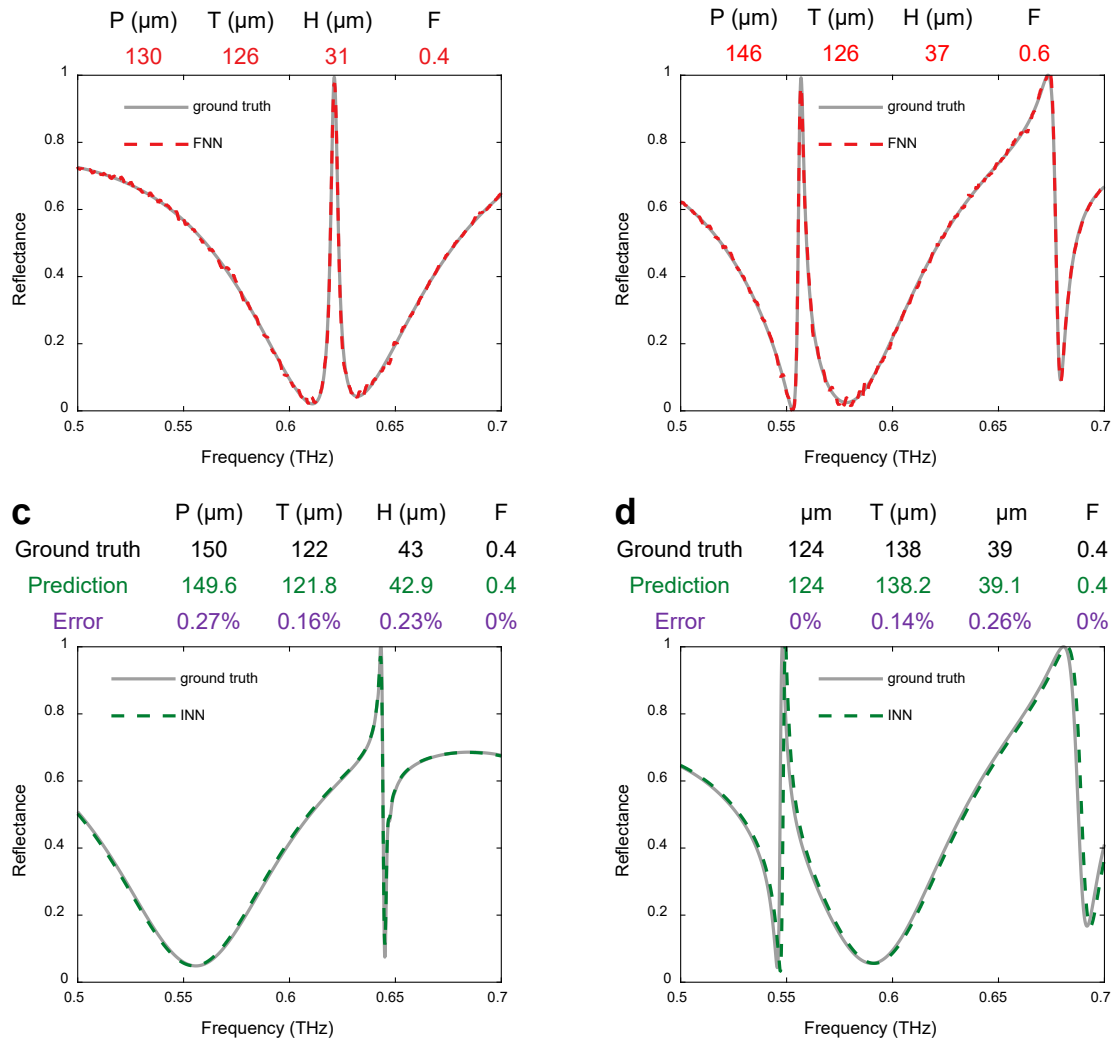

Figure 2. Evaluation of the DL model. (a,b) Spectra predicted by FNN and the corresponding ground truth by optical simulation. (c,d) Spectra of ground truth and INN design for randomly selected test samples. The green dashed spectra correspond to the predicted metastructures by INN.

Based on the high performance of FNN and INN, we combine them to construct a trained bidirectional network for the smart design of diverse THz fingerprint metasensors. Here, we give the metasensor design paradigms of two common analytes, namely α-santonin and α-lactose, who have the fingerprint feature frequencies in the THz band from 0.5 THz to 0.7 THz (see more details in **Figure** S2, Supporting Information) [21, 22]. The design is based on the angular multiplexing of IAM [17], in which a sequence of reflectance spectra with resonance

peaks should be determined by a succession of incident angles of THz wave. In view of the setup for angle-resolved THz spectroscopy, the operational incident angles in experiments are usually within the range from 16° to 56° due to the practical limit. Typically, the resonance peak of IAM should have a shift towards lower frequencies with the increased angle.[21] In order to enable the powerful INN design, one can provide a reflectance spectrum with the resonance peak working at the central angle of 36°, according to the frequency location of the analyte fingerprint feature. With the aim to obtain the IAM structure parameters, one can tune the customer-defined blue dots on the spectral layout to match the resonance peak position with the fingerprint frequency point, as shown in **Figure** 3a,b. The designed metasensors demonstrate the spectral resonance frequencies of 0.630 THz and 0.529 THz at the incident angle of 36° for α-santonin and α-lactose, respectively, which match well with their fingerprint feature positions. By using the designed metastructures, one can further obtain two sets of reflectance spectra with sequential resonance peaks of IAM, as observed in **Figure** 3c(i), d(i). Under the scheme of angle multiplexing, the peak envelopes for the two sets of spectra can be used as the background signals of metasensors without any analyte loading. When the samples of α-santonin and α-lactose with the same thickness of 8 μm are coated on the flat sensing surface of the two metasensors, respectively, the decline for the two sets of peak envelopes can be clearly observed in **Figure** 3c(ii), d(ii). The corresponding fingerprint signals $A=|R_A-R_0|$ can be retrieved by comparing the envelope changes R_0 and R_A before and after sample loading, as shown in **Figure** 3c(iii), d(iii). In comparison with the conventional method by simulation, the retrieved fingerprint signals by IAM sensors can successfully demonstrate the significant peak frequencies around 0.63 THz and 0.53 THz, respectively, which imply that the trace α-santonin and α-lactose could be well detected by our design approach. Therefore, our DL design suggests great potential for the smart design of THz fingerprint metasensors.

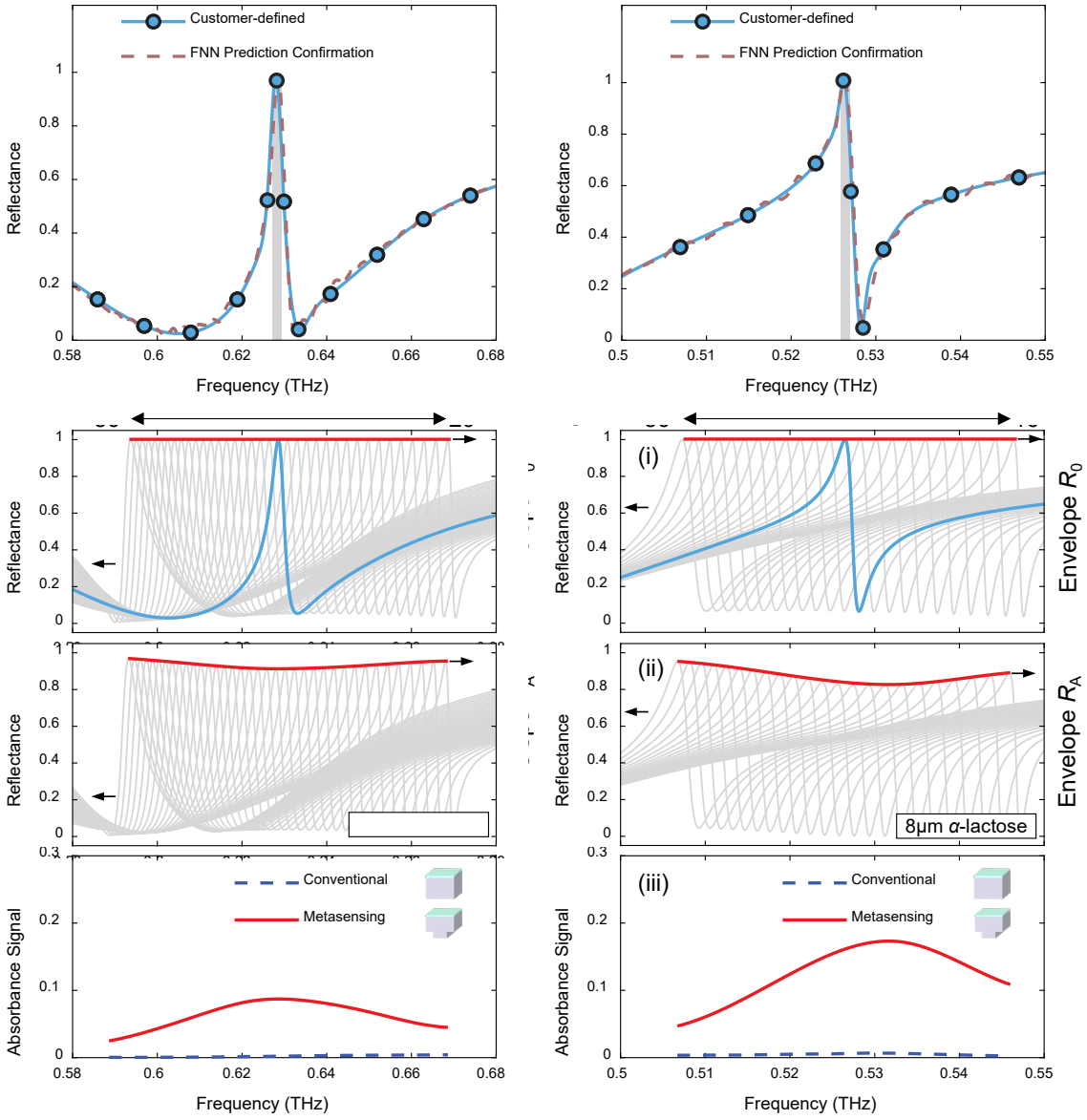

Figure 3 (a) and (b) are spectra fitted by freely movable blue dots for θ=36°, which contains the specific peak frequencies of 0.630 THz and 0.529 THz for the fingerprints of α-santonin and α-lactose, respectively.They are used as the input of INN to predict metastructure parameters, which are confirmed by spectra predicted by the FNN. (c) and (d) are multiplexing detection results for α-santonin and α-lactose, respectively, where (i) and (ii) denote angle-multiplexed reflectance spectra with their peak envelopes before and after trace sample loading, and (iii) represents retrieved fingerprint by metasensing compared to conventional measurement.

2.3. DL-guided IAM experiments for trace THz fingerprint sensing

According to the DL design in **Figure** 3b, we conduct the IAM experiments for THz angle-multiplexed metasensing of trace α-lactose powder. The experimental system employs a

reflection-type THz time-domain spectroscopy (THz-TDS) with a tunable angle configuration, as illustrated in **Figure** 4a. Here the characterization by scanning electron microscope (SEM) demonstrates that the fabricated IAM has a flat sensing surface along with a uniform depth-to-width ratio for periodic gratings underneath. We measure the time-domain signals of bare and analyte-loaded IAMs under the excitation of TE wave for each incident angle, as shown in **Figure** 4b. These signals are converted to the frequency-domain signals by fast Fourier transform, as observed in **Figure** 4c. The frequency-domain signals can be used to calculate a series of angle-resolved reflectance spectra with their peak envelopes shown in **Figure** 4d,e,f. These figures indicate the envelope curves for trace α-lactose coatings of 20.4 μg/mm² and 40.8 μg/mm² show distinct decline levels in comparison with that of uncoated IAM. Particularly, the experimental signal intensity deviation from simulation results in Figure 3d could be attributed to fabrication size errors and frequency sampling discrepancies. Despite this, the retrieved fingerprint spectra of α-lactose in Figure 4g clearly exhibit the specific peak at the frenquency of 0.529 THz. This sensing performance is much better than the conventional approach, which is unable to identify the featured fingerprint peak. At the specific frequency point of 0.529 THz, the absorption intensities of α-lactose elevate from 1.3% and 3.1% in conventional way to 12.1% and 17.7% for the trace coatings of 20.4 μg/mm² and 40.8 μg/mm², respectively. The exparimental data of IAM fingerpirnt sensing indicates good agreement with the smart design result in Figure 3d.

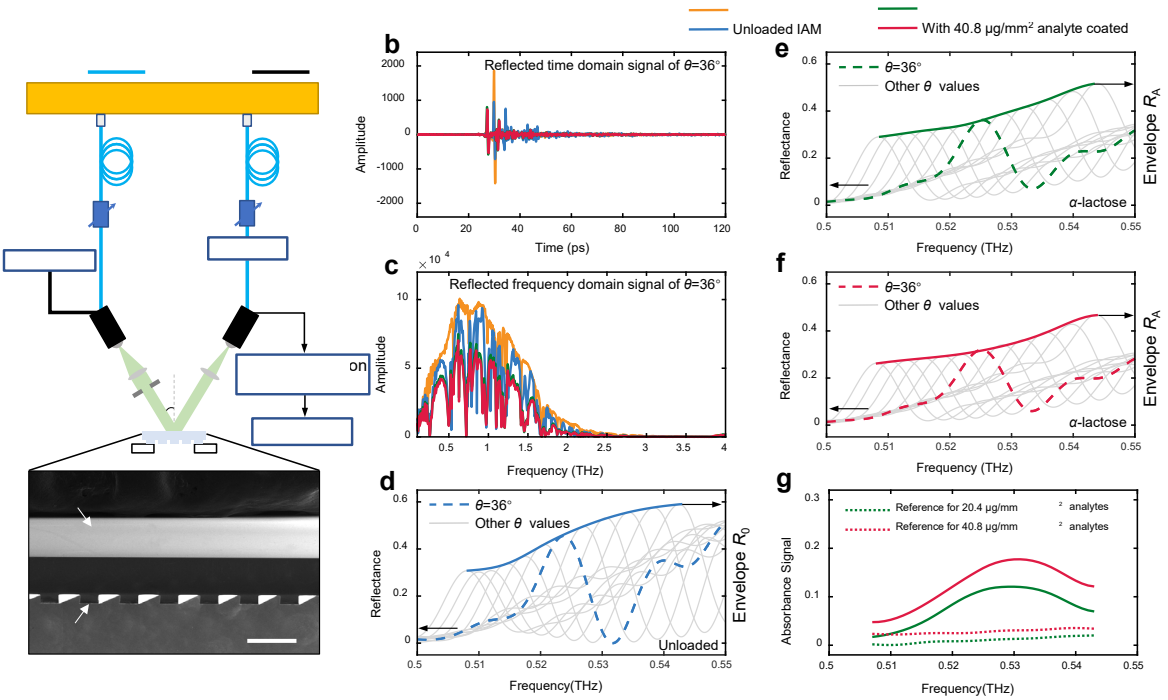

Figure 4. DL-guided IAM experiments for trace THz fingerprint sensing. (a) Schamatic drawing of reflection-mode angle-multiplexed THz-TDS platform and SEM image of IAM. Reflected (b) time and (c) frequency domain signals, where θ=36°. Angle-multiplexed reflectance spectra and the corresponding peak envelope signal of (d) bare IAM, (e) IAM with 20.4 μg/mm² α-lactose coated and (f) IAM with 40.8 μg/mm² α-lactose, where θ changes from 26° to 48° with the angle step of 2°. (g) Retrieved fingerprint absorbance signal of α-lactose.

We compare the performance of our method with some previous studies in Table 1. As presented, our metasensor demonstrates considerable performance improvement with peak enhancement of 9.3-fold for 20.4 μg/mm² α-lactose, which is higher than other reported experimental results. We adopt deep learning in combination with smart simulation to guide the experiments, which is highly efficient and much more advanced than conventional methods based on brute-force simulations. The experimental results validte the reliability and superiority of our methodology in trace THz fingerprint metasensing. Our study will provide a paradigm for other THz metasensor design based on artificial intelligence.

Table 1 Performance comparison between our investigation and other studies.

Ref.	Structure	Frequency range	Analyte	Multiplexed Scheme	Design Method	Time	Enhancing times
[44]	Metagrating	Mid-IR	cBN	Angle	Brute-force simulation	Several days/weaks	~5.4(simulated)
[17]	Metagrating	THz	α-lactose	Angle	Brute-force simulation	Several days/weaks	~13(simulated)
[18]	Plasmonic metasurface	THz	glucose	Graphene-voltage/Geometry	Brute-force simulation	Several days/weaks	~5(simulated)
[19]	Plasmonic metasurface	THz	α-lactose	Geometry	Brute-force simulation	Several days/weaks	~7.3(measured)
Our work	IAM	THz	α-lactose	Angle	Deep learning & Smart simulation	Several hours	~9.3(measured)

3. Conclusion

In summary, we establish a cascaded neural network for rapid and intelligent design of metasensor for trace THz fingerprint detection. According to the fingerprint spectrum of trace sample, one can define the target spectrum of IAM with a flat sensing surface and use the DL model to deduce the corresponding metastructure parameters. By the angle multiplexing technique, we achieve THz fingerprint sensing of trace α-lactose. The experimental detection limit is 20.4 μg/mm^2 with the enhacing time of 9.3. Our research provides a powerful software tool to guide the quick smart design of trace THz metasensing, and will also facilitate the high-efficiency development of other THz metadevices and metasystems.

4. Appendix A: Material and Methods

Sample Fabrication: In the begining, a 2-inch silicon wafer with the thickness of 200 μm is prepared and cleaned using acetone, ethanol and deionized water. The all-dielectric metagrating is fabricated by photolithography and inductively coupled plasma etching on the wafer. The morphology of metagrating is characterized by scanning electron microscopy (SEM, SIGMA HD, Carl Zeiss, Germany).

THz Measurement: A commercial THz-TDS system (QT-TS2000, Quenda Terahertz Technologies Co., Ltd, Qingdao, China) is used to measure the angle-multiplexed spectra of samples. The system has a working frequency range from 0.1 to 4.0 THz, and its frequency

resolution and signal-to-noise ratio are ~8 GHz and >70 dB, respectively. The measurement is carried out in dry air with collimated light incidence. The THz spot diameter under normal incidence is confined to 2 cm by an optical diaphragm. In the measurement, the THz time-domain spectra of a gold mirror reference and all tested samples are measured five times. In the reflection-mode angle-multiplexed platform, two sets of the photoconductive antenna (PCA) are applied. For each scanning angle, we adopt the reflected signal of incident THz laser pulse from a standard gold mirror as the reference signal. Afterward, we measure the reflected THz signals for the bare metagrating and the analyte-loaded metagrating, respectively. During the whole process, the angle interval of 2° is used to improve the detection efficiency.

Numerical Simulations: To perform the full-wave simulation of metagrating, the rigorous coupled-wave analysis (RCWA) and the finite element method (FEM) based on the commercial software Comsol Multiphysics are adopted.[45] The RCWA is performed as an efficient code-based frequency-domain numerical modeling tool, which can quickly simulate optical spectra of various metagratings. The FEM is mainly used for the validation of RCWA-based results and field distribution analysis. During the FEM simulation, the Floquet periodic boundary conditions are applied for the infinite metaunits of metagrating, the adaptive inhomogeneous triangle meshing is used to discretize the physical model. In the optical simulation, the refractive index of silicon is assumed to be 3.44 within the investigated THz frequency range.

Data Collection: A total of 18018 data instances are generated randomly as the training samples. 2000 data instances not existing in the training sampling space are used as the testing samples (Windows10 operation system, GeForce GTX 3080Ti GPU, Intel(R) Core(TM) i7-10700K CPU @ 3.80 GHz 3.79 GHz and 16GB of RAM).

Acknowledgements

This work was supported by NSAF (U2130112), NSFC (62175205), the Natural Science Foundation of Fujian Province (2020J06009), Youth Talent Support Program of Fujian

Province (Eyas Plan of Fujian Province) [2022] and the Shenzhen Science and Technology Development Funds under Grant (JCYJ20220530143015035). In addition, Z.D. would like to acknowledge the funding support by Agency for Science, Technology and Research (A*STAR) under its AME IRG (Project No. A20E5c0093), Career Development Award grant (Project No. C210112019), <MTC IRG (Project No. M21K2c0116 & M22K2c0088), DELTA-Q 2.0 (Project No. C230917005), and Quantum Engineering Programme 2.0 (Award No. NRF2021-QEP2-03-P09).

Declaration of competing interest

The authors declare that they have no known competing financial interests or personal relationships that could have appeared to influence the work reported in this paper.

Supporting Information

Supporting Information is available from the Wiley Online Library or from the author.

Received:

Revised:

Published online:

References

1. P. Wang, J. Lou, G. Fang, and C. Chang, "Progress on cutting-edge infrared-terahertz biophysics," IEEE Trans. Microwave Theory Tech. **70**, 5117-5140 (2022).
2. Y. Peng, C. Shi, Y. Zhu, M. Gu, and S. Zhuang, "Terahertz spectroscopy in biomedical field: a review on signal-to-noise ratio improvement," PhotoniX **1**, 1-18 (2020).
3. T. Nagatsuma, G. Ducournau, and C. C. Renaud, "Advances in terahertz communications accelerated by photonics," Nat. Photonics **10**, 371-379 (2016).
4. R. I. Stantchev, B. Sun, S. M. Hornett, P. A. Hobson, G. M. Gibson, M. J. Padgett, and E. Hendry, "Noninvasive, near-field terahertz imaging of hidden objects using a single-pixel detector," Sci. Adv. **2**, e1600190 (2016).

5. X. Yang, X. Zhao, K. Yang, Y. Liu, Y. Liu, W. Fu, and Y. Luo, "Biomedical applications of terahertz spectroscopy and imaging," Trends Biotechnol. **34**, 810-824 (2016).
6. W. J. Choi, K. Yano, M. Cha, F. M. Colombari, J.-Y. Kim, Y. Wang, S. H. Lee, K. Sun, J. M. Kruger, A. F. de Moura, and N. A. Kotov, "Chiral phonons in microcrystals and nanofibrils of biomolecules," Nat. Photonics **16**, 366-373 (2022).
7. R. Damari, O. Weinberg, D. Krotkov, N. Demina, K. Akulov, A. Golombek, T. Schwartz, and S. Fleischer, "Strong coupling of collective intermolecular vibrations in organic materials at terahertz frequencies," Nat. Commun. **10**, 3248 (2019).
8. M. Gupta and R. Singh, "Terahertz sensing with optimized Q/Veff metasurface cavities," Adv. Opt. Mater. **8**, 1902025 (2020).
9. W. Xu, L. Xie, J. Zhu, W. Wang, Z. Ye, Y. Ma, C.-Y. Tsai, S. Chen, and Y. Ying, "Terahertz sensing of chlorpyrifos-methyl using metamaterials," Food Chem. **218**, 330-334 (2017).
10. K. Yang, J. Li, M. L. de la Chapelle, G. Huang, Y. Wang, J. Zhang, D. Xu, J. Yao, X. Yang, and W. Fu, "A terahertz metamaterial biosensor for sensitive detection of microRNAs based on gold-nanoparticles and strand displacement amplification," Biosens. Bioelectron. **175**, 112874 (2021).
11. Z. Zhang, C. Zhong, F. Fan, G. Liu, and S. Chang, "Terahertz polarization and chirality sensing for amino acid solution based on chiral metasurface sensor," Sensor. Actuat. B-Chem. **330**, 129315 (2021).
12. X. Zhan, S. Yang, G. Huang, L. Yang, Y. Zhang, H. Tian, F. Xie, M. L. de la Chapelle, X. Yang, and W. Fu, "Streptavidin-functionalized terahertz metamaterials for attomolar exosomal microRNA assay in pancreatic cancer based on duplex-specific nuclease-triggered rolling circle amplification," Biosens. Bioelectron. **188**, 113314 (2021).
13. A. Ahmadivand, B. Gerislioglu, Z. Ramezani, A. Kaushik, P. Manickam, and S. A. Ghoreishi, "Functionalized terahertz plasmonic metasensors: Femtomolar-level detection of SARS-CoV-2 spike proteins," Biosens. Bioelectron. **177**, 112971 (2021).
14. C. Zhang, T. Xue, J. Zhang, L. Liu, J. Xie, G. Wang, J. Yao, W. Zhu, and X. Ye, "Terahertz toroidal metasurface biosensor for sensitive distinction of lung cancer cells," Nanophotonics **11**, 101-109 (2022).
15. R. Wang, L. Xu, L. Huang, X. Zhang, H. Ruan, X. Yang, J. Lou, C. Chang, and X. Du, "Ultrasensitive Terahertz Biodetection Enabled by Quasi-BIC-Based Metasensors," Small, 2301165 (2023).
16. A. Leitis, A. Tittl, M. Liu, B. H. Lee, M. B. Gu, Y. S. Kivshar, and H. Altug, "Angle-multiplexed all-dielectric metasurfaces for broadband molecular fingerprint retrieval," Sci. Adv. **5**, eaaw2871 (2019).
17. J. Zhu, S. Jiang, Y. Xie, F. Li, L. Du, K. Meng, L. Zhu, and J. Zhou, "Enhancing terahertz molecular fingerprint detection by a dielectric metagrating," Opt. Lett. **45**, 2335-2338 (2020).
18. L. Sun, L. Xu, J. Wang, Y. Jiao, Z. Ma, Z. Ma, C. Chang, X. Yang, and R. Wang, "A pixelated frequency-agile metasurface for broadband terahertz molecular fingerprint sensing," Nanoscale **14**, 9681-9685 (2022).
19. J. Lyu, S. Shen, L. Chen, Y. Zhu, and S. Zhuang, "Frequency selective fingerprint sensor: the Terahertz unity platform for broadband chiral enantiomers multiplexed signals and narrowband molecular AIT enhancement," Photonix **4**, 28 (2023).
20. X. Liu, W. Chen, Y. Ma, Y. Xie, J. Zhou, L. Zhu, Y. Xu, and J. Zhu, "Enhancing THz fingerprint detection on the planar surface of an inverted dielectric metagrating," Photonics Res. **10**, 2836-2845 (2022).

21. Y. Xie, X. Liu, J. Zhou, H. Zhang, J.-Y. Lin, W. Chen, L.-G. Zhu, K. Meng, Q. H. Liu, and J. Zhu, "Enhancing Trace Terahertz Fingerprint Sensing by the Lossy Silicon Metagrating With a Gold Mirror," IEEE Trans. Microwave Theory Tech. (2023).
22. Y. Xie, Y. Ma, X. Liu, S. A. Khan, W. Chen, L. Zhu, J. Zhu, and Q. H. Liu, "Dual-degree-of-freedom multiplexed metasensor based on quasi-BICs for boosting broadband trace isomer detection by thz molecular fingerprint," IEEE J. Sel. Top. Quantum Electron. **29**, 8600110 (2023).
23. I. Malkiel, M. Mrejen, A. Nagler, U. Arieli, L. Wolf, and H. Suchowski, "Plasmonic nanostructure design and characterization via deep learning," Light Sci. Appl. **7**, 60 (2018).
24. S. An, C. Fowler, B. Zheng, M. Y. Shalaginov, H. Tang, H. Li, L. Zhou, J. Ding, A. M. Agarwal, and C. Rivero-Baleine, "A deep learning approach for objective-driven all-dielectric metasurface design," ACS Photonics **6**, 3196-3207 (2019).
25. S. So, T. Badloe, J. Noh, J. Bravo-Abad, and J. Rho, "Deep learning enabled inverse design in nanophotonics," Nanophotonics **9**, 1041-1057 (2020).
26. W. Ma, Z. Liu, Z. A. Kudyshev, A. Boltasseva, W. Cai, and Y. Liu, "Deep learning for the design of photonic structures," Nat. Photonics **15**, 77-90 (2021).
27. N. J. Dinsdale, P. R. Wiecha, M. Delaney, J. Reynolds, M. Ebert, I. Zeimpekis, D. J. Thomson, G. T. Reed, P. Lalanne, and K. Vynck, "Deep learning enabled design of complex transmission matrices for universal optical components," ACS Photonics **8**, 283-295 (2021).
28. J. Peurifoy, Y. Shen, L. Jing, Y. Yang, F. Cano-Renteria, B. G. DeLacy, J. D. Joannopoulos, M. Tegmark, and M. Soljačić, "Nanophotonic particle simulation and inverse design using artificial neural networks," Sci. Adv. **4**, eaar4206 (2018).
29. L. Li, H. Ruan, C. Liu, Y. Li, Y. Shuang, A. Alù, C.-W. Qiu, and T. J. Cui, "Machine-learning reprogrammable metasurface imager," Nat. Commun. **10**, 1082 (2019).
30. Z. Liu, D. Zhu, S. P. Rodrigues, K.-T. Lee, and W. Cai, "Generative model for the inverse design of metasurfaces," Nano Lett. **18**, 6570-6576 (2018).
31. W. Chen, Y. Gao, Y. Li, Y. Yan, J. Y. Ou, W. Ma, and J. Zhu, "Broadband solar metamaterial absorbers empowered by transformer‐based deep learning," Adv. Sci. **10**, 2206718 (2023).
32. J. Xiong, J. Shen, Y. Gao, Y. Chen, J. Y. Ou, Q. H. Liu, and J. Zhu, "Real‐Time On‐Demand Design of Circuit‐Analog Plasmonic Stack Metamaterials by Divide‐and‐Conquer Deep Learning," Laser Photonics Rev. **17**, 2100738 (2023).
33. E. Khoram, Z. Wu, Y. Qu, M. Zhou, and Z. Yu, "Graph Neural Networks for Metasurface Modeling," ACS Photonics **10**, 892-899 (2022).
34. W. Chen, Y. Li, Y. Liu, Y. Gao, Y. Yan, Z. Dong, and J. Zhu, "All-Dielectric Sers Metasurface with Strong Coupling Quasi-BIC Energized by Transformer-Based Deep Learning," Adv. Opt. Mater., 2301697.
35. X. Han, Z. Fan, Z. Liu, C. Li, and L. J. Guo, "Inverse design of metasurface optical filters using deep neural network with high degrees of freedom," InfoMat **3**, 432-442 (2021).
36. W. Xi, Y.-J. Lee, S. Yu, Z. Chen, J. Shiomi, S.-K. Kim, and R. Hu, "Ultrahigh-efficient material informatics inverse design of thermal metamaterials for visible-infrared-compatible camouflage," Nat. Commun. **14**, 4694 (2023).
37. B. Qin, Y. Zhu, Y. Zhou, M. Qiu, and Q. Li, "Whole-infrared-band camouflage with dual-band radiative heat dissipation," Light Sci. Appl. **12**, 246 (2023).
38. C. Qian, B. Zheng, Y. Shen, L. Jing, E. Li, L. Shen, and H. Chen, "Deep-learning-enabled self-adaptive microwave cloak without human intervention," Nat. Photonics **14**, 383-390 (2020).

39. D. Liu, Y. Tan, E. Khoram, and Z. Yu, "Training deep neural networks for the inverse design of nanophotonic structures," ACS Photonics **5**, 1365-1369 (2018).
40. L. Gao, X. Li, D. Liu, L. Wang, and Z. Yu, "A bidirectional deep neural network for accurate silicon color design," Adv. Mater. **31**, 1905467 (2019).
41. R. Unni, K. Yao, and Y. Zheng, "Deep convolutional mixture density network for inverse design of layered photonic structures," ACS Photonics **7**, 2703-2712 (2020).
42. J. L. Bentley, "Multidimensional divide-and-conquer," Commun. ACM **23**, 214-229 (1980).
43. P. Zhuang and X. Ding, "Divide-and-conquer framework for image restoration and enhancement," Eng. Appl. Artif. Intell. **85**, 830-844 (2019).
44. Y. Xie, X. Liu, F. Li, J. Zhu, and N. Feng, "Ultra-wideband enhancement on mid-infrared fingerprint sensing for 2D materials and analytes of monolayers by a metagrating," Nanophotonics **9**, 2927-2935 (2020).
45. J. Qiu, X. Liu, Z. Liang, and J. Zhu, "Ultra-wideband perfect reflection and tunneling by all-dielectric metamaterials," Opt. Lett. **46**, 849-852 (2021).